Engineering

Industrial & Management Engineering fields

Okayama University *Year* 1995

Visual servoing with hand-eye manipulator-optimal control approach

Koichi Hashimoto
Okayama University

Takumi Ebine
The Defence Agency

Hidenori Kimura
University of Tokyo

negative definite function. Therefore, we conclude global asymptotic stability by invoking the Lyapunov's direct method (see e.g. [29]).

REFERENCES

[1] S. W. Wijesoma, D. F. H. Wolfe and R. J. Richards, "Eye-to-hand coordination for vision-guided robot control applications," *Int. J. Robot. Res.*, vol. 12, no. 1, pp. 65–78, 1993.

[2] A. J. Koivo and N. Houshangi, "Real-time vision feedback for servoing robotic manipulators with self-tuning controller," *IEEE Trans. Syst., Man, Cybern.*, vol. 21, no. 1, Jan./Feb. 1991, pp. 134–142.

[3] P. K. Allen, A. Timcenko, B. Yoshimi and P. Michelman, "Automated tracking and grasping of a moving object with a robotic hand-eye system," *IEEE Trans. Robot. Automat.*, vol. 9, no. 2, pp. 152–165, Apr. 1993.

[4] M. Lei and B. K. Ghosh, "Visually guided robotic tracking and grasping of a moving object," *Proc. 32nd Conf. on Decision and Control*, San Antonio, TX, Dec. 1993, pp. 1604–1609.

[5] G. D. Hager, W. C. Chang and A. S. Morse, "Robot hand-eye coordination based on stereo vision," *IEEE Contr. Syst. Mag.*, vol. 15, no. 1, Feb. 1995, pp. 30–39.

[6] F. Miyazaki and Y. Masutani, "Robustness of sensory feedback control based on imperfect Jacobian," *Robotics Research: The Fifth International Symposium*, H. Miura and S. Arimoto, Eds. Cambridge, MA: MIT Press, 1990, pp. 201–208.

[7] L. E. Weiss, A. C. Sanderson and C. P. Neuman, "Dynamic sensor-based control of robots with visual feedback," *IEEE J. Robot. Automat.*, vol. 3, no. 9, pp. 404–417, 1987.

[8] K. Hashimoto, T. Kimoto, T. Ebine and H. Kimura, "Manipulator control with image-based visual servo," in *IEEE Int. Conf. Robotics and Automation*, Sacramento, CA., pp. 2267–2272, 1991.

[9] J. T. Feddema, C. S. G. Lee and O. R. Mitchell, "Weighted selection of image features for resolved rate visual feedback control," *IEEE Trans. Robot. Automat.*, vol. 7, no. 1, pp. 31–47, Feb. 1991.

[10] H. Hashimoto, T. Kubota, M. Sato and F. Harashima, "Visual control of robotic manipulator based on neural networks," *IEEE Trans. Ind. Electron.*, 1992, vol. 9, no. 6, pp. 490–496.

[11] B. Espiau, F. Chaumette, and P. Rives, "A new approach to visual servoing in robotics," *IEEE Trans. Robot. Automat.*, vol. 8, no. 3, pp. 313–326, June 1992.

[12] N. P. Papanikolopoulos, P. Khosla, and T. Kanade, "Visual tracking of a moving target by a camera mounted on a robot: A combination of control and vision," *IEEE Trans. Robot. Automat.*, 1993, vol. 9, no. 1, pp. 14–35.

[13] N. P. Papanikopoulos and P. K. Khosla, "Adaptive robotic visual tracking: Theory and experiments," *IEEE Trans. Automat. Contr.*, vol. 38, no. 3, Mar. 1993, pp. 429–444.

[14] K. Hashimoto and H. Kimura, "Dynamic visual servoing with nonlinear model-based control," *1993 IFAC World Cong.*, Sydney, Australia, vol. 9, July 1993, pp. 405–408.

[15] R. Carelli, O. Nasisi, and B. Kuchen, "Adaptive robot control with visual feedback," in *Proc. Amer. Control Conf.*, Baltimore, MD, June 1994, pp. 1757–1760.

[16] K. Hashimoto, T. Inoue, T. Ebine, and H. Kimura, "Visual servoing based on adaptive identifier," in *Proc. 1994 Japan-USA Symp. Flexible Automation*, July 1994, Kobe, Japan, pp. 39–42.

[17] A. Castaño and S. Hutchinson, "Visual compliance: Task-directed visual servo control," *IEEE Trans. Robot. Automat.*, vol. 10, no. 3, June 1994, pp. 334–342.

[18] V. W. Chen and R. H. Cannon, "Experiments in nonlinear adaptive control of multi-manipulator free-flying robots," in *Proc. IEEE Int. Conf. Robotics and Automation*, San Diego, CA, May 8–14, 1994, pp. 2213–2220.

[19] G. Hager, S. Hutchinson, and P. Corke, "A tutorial on visual servo control," *Tutorial TT3, IEEE Int. Conf. Robotics and Automation*, Apr. 1996, Minneapolis, MN.

[20] M. Takegaki and S. Arimoto, "A new feedback method for dynamic control of manipulators," *ASME J. Dyn. Syst., Meas., Contr.*, vol. 102, June 1981, pp. 119–125.

[21] D. E. Koditschek, "Natural control of robot arms," Rep. 8409, Center for Systems Science, Yale University, New Haven, CT, Dec. 1984 (rev'd Feb. 1985).

[22] S. Arimoto, F. Miyazaki, H. G. Lee, and S. Kawamura, "Rivival of Lyapunov's direct method in robot control and design," in *Proc. Amer. Control Conf.*, Atlanta, GA., June 1988, pp. 1764–1769.

[23] J. J. Craig, *Introduction to Robotics: Mechanics and Control*, 2nd ed. Reading, MA: Addison Wesley, 1989.

[24] F. Miyazaki and S. Arimoto, "Sensory feedback for robot manipulators," *J. Robot. Syst.*, vol. 2, no. 1, 1985, pp. 53–71.

[25] R. Kelly and A. Marquez, "Fixed-eye direct visual feedback control of planar robots," *J. Syst. Eng.*, vol. 4, no. 5, Nov. 1995, pp. 239–248.

[26] D. Koditschek, "Natural motion for robot arms," in *Proc. 23rd Conf. Decision and Control*, Las Vegas, NV, Dec. 1984, pp. 733–735.

[27] R. K. Lenz and R. Y. Tsai, "Techniques for calibration of the scale factor and image center for high accuracy 3-D machine vision metrology," *IEEE Trans. Pattern Anal. Machine Intell.*, vol. 10, no. 5, Sept. 1988, pp. 713–720.

[28] I. D. Faux and M. J. Pratt, *Computational Geometry for Design and Manufacturing*. New York: Ellis-Horwood, 1985, pp. 81–84.

[29] M. Vidyasagar, *Nonlinear Systems Analysis*. Englewood Cliffs, NJ: Prentice Hall, 1993.

[30] D. E. Koditschek, "Some applications of natural motion control," *Trans. ASME J. Dyn. Syst., Meas., Contr.*, vol. 113, Dec. 1991, pp. 552–557.

[31] R. Kelly, P. Shirkey and M. W. Spong, "Fixed camera visual servo control for planar robots," *1996 IEEE Int. Conf. Robotics and Automation*, Apr. 22–28, 1996, Minneapolis, MN, vol. 3, pp. 2643–2649.

[32] R. Y. Tsai, "A versatile camera calibration technique for high-accuracy 3D machine vision metrology using off-the-shelf TV cameras and lenses," *IEEE J. Robot. Automat.*, vol. RA-3, no. 4, Aug. 1987, pp. 323–344.

[33] B. E. Bishop, "Real-time visual servo with application to the acrobot," M.S. Thesis, University of Illinois, Urbana-Champaign, 1994.

[34] M. Rosenlicht, *Introduction to Analysis*. New York: Dover, New York, 1968.

[35] M. W. Spong and M. Vidyasagar, *Robot Dynamics and Control*. New York: Wiley.

[36] T. Ozaki, T. Suzuki, T. Furuhashi, S. Okuma, and Y. Uchikawa, "Trajectory control of robotic manipulators using neural networks," *IEEE Trans. Ind. Electron.*, 1991, vol. 38, no. 3, pp. 195–202.

Visual Servoing with Hand-Eye Manipulator—Optimal Control Approach

Koichi Hashimoto, Takumi Ebine, and Hidenori Kimura

***Abstract*—This paper proposes a control theoretic formulation and a controller design method for the feature-based visual servoing with redundant features. The linear time-invariant (LTI) formulation copes with the redundant features and provides a simple framework for controller design. The proposed linear quadratic (LQ) method can deal with the redundant features, which is important because the previous LQ methods are not applicable to redundant systems. Moreover, this LQ method gives flexibility for performance improvement instead of the very limited design parameters provided by the generalized inverse and task function controllers. Validity of the LTI model and effectiveness and flexibility of the LQ optimal controller are evaluated by real-time experiments on a PUMA 560 manipulator.**

Manuscript received August 17, 1994; revised August 3, 1995. This paper was recommended for publication by Associate Editor K. Ikeuchi and Editor S. E. Salcudean upon evaluation of reviewers' comments.

K. Hashimoto is with the Department of Systems Engineering, Okayama University, Okayama 700, Japan.

T. Ebine is with the Defence Agency, Tokyo 153, Japan.

H. Kimura is with the Department of Mathematical Engineering and Information Physics, University of Tokyo, Tokyo 113, Japan.

Publisher Item Identifier S 1042-296X(96)00491-0.

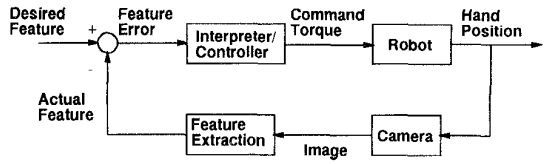

Fig. 1. Block diagram of feature-based visual feedback.

I. Introduction

Visual feedback is a prevalent approach in autonomous manipulation. Conventional visual feedback schemes, e.g., [1], used the visual sensor to generate the hand trajectory at the stage of environment inspection. The whole manipulation was completely based on the generated hand trajectory. This off-line planning approach is useful for structured environments. However, in dynamically changing environments, visual sensors should be incorporated in the feedback loop because real-time recognition of the environment is necessary.

Control schemes which utilize the visual sensors in the feedback loop are called *visual servo systems* [2]. Visual servoing schemes are classified into two groups, namely, *position-based* and *feature-based*. Position-based approaches, e.g., [3]–[5], estimate/predict the object position and orientation in real-time and use the information to generate the hand trajectory. Koivo and Houshangi [3] introduced the autoregressive type object position predictor and proposed a self-tuning controller to grasp an object. Allen *et al.* [4] used an α-β-γ filter to predict the hand position tracking the moving object. Wilson [5] used Kalman filter to estimate the relative position and orientation between the camera and the object.

Feature-based approach was proposed by Weiss *et al.* in 1987 [6] and is being studied by many authors. The feature-based approach uses the object features directly in the visual sensory output without computing the object position and orientation. Fig. 1 shows a block diagram of the feature-based approach. Most research on the feature-based approach is based on the *Jacobian of ideal inverse interpretation* to interpret the feature error. The Jacobian is defined in [6] and considered as the infinitesimal change of the features according to the infinitesimal change of the relative position and orientation between the camera and the object. These results have shown so far that, if the features are selected appropriately, feature-based control schemes work well. However, an inevitable and important problem in control, *controllability*, has never been treated formally. The following are examples of the previous work on the feature-based approach.

Weiss *et al.* [6] and Feddema *et al.* [7], [8] have studied the selection method of the features to make the Jacobian have good condition. Real-time experiments of gasket tracking showed that the properly selected features are necessary to minimize the effect of image noise [8]. However, the controllability problem was not considered because the smallest set of the features were selected to make the visual feedback system controllable. Papanikolopoulos *et al.* [9] introduced sum-of-squared differences (SSD) optical flow and experimentally examined many control algorithms including proportional and integral (PI), pole assignment, and linear quadratic Gaussian (LQG). An adaptive control scheme was also examined in [10]. However, the controllability problem was not considered because their formulation was also based on the minimum set of features. Espiau *et al.* [11] introduced the concept of task function and used the interaction matrix and its generalized inverse to derive the desired velocity of the hand. They showed a stability condition and an experiment of four point, i.e., redundant features, tracking but their control parameter was only a scalar λ. Thus their task function approach was not very attractive to maximize the tracking performance. Jang and Bien [12] mathematically defined the concept of *feature* and derived the feature Jacobian matrix. They used the generalized inverse of the feature Jacobian and proportional plus integral plus derivative (PID) control to generate the hand trajectory. No problem arose from the redundant features because the generalized inverse matrix gives a least square error solution if the exact solution does not exist. Although this is a simple way to avoid the controllability problem, it was not interesting from the control point of view because no parameter was introduced to improve the performance. The authors [13], [14] derived the *image Jacobian* which is a special case of the Jacobian of ideal inverse interpretation and used the generalized inverse of the image Jacobian. A comparison between the position-based and feature-based control schemes was made by simulating and doing object tracking experiments. However, no discussion was done on controllability.

This paper discusses the controllability of the visual servo system with redundant features. The system is linearized at the desired point yielding a linear time-invariant (LTI) multi-input multi-output (MIMO) model. The image features are considered as state variables and the joint velocities are considered as control inputs. If the number of features exceeds the number of joints, the LTI model becomes uncontrollable. Since the LTI model allows each state variables to move independently, which means object deformation, the redundancy of the features makes the system uncontrollable. However, if the reference image is generated properly, the desired features should be reachable because the object is rigid. Thus posing some restrictions on the state variables makes the system controllable. Therefore, we decompose the state variables into controllable and uncontrollable modes and, as a result, we can prove the local reachability of the LTI system by using this state decomposition.

We also propose an optimal approach to the design of the feedback controller. Since the system is uncontrollable, the conventional design procedure does not work well. Thus we utilize the mode decomposition and derive the optimal controller that minimizes an linear quadratic (LQ) performance index. The controller becomes LTI state feedback with the state being the object features. Therefore, none of the computations of the depth, image Jacobian nor its generalized inverse is required. This is a favorable characteristic of the proposed LTI optimal approach.

To evaluate the validity of the proposed LTI model and the optimal controller, real-time experiments on PUMA 560 arm have been carried out. Translational and rotational step experiments demonstrate fast response. The tracking experiments show that the performance can be easily tuned by changing the weight matrices. These experiments show the effectiveness of the proposed optimal control approach.

This paper is organized as follows. In Section II we briefly review the discrete time LTI model. Section III proposes the optimal controller design method. The controllability of the LTI model is also discussed in this section. Section IV outlines our experimental setup and gives experimental results. Discussion on control performance is presented here. We conclude our results in Section V.

II. Image Jacobian and LTI Model

In general, rich feedback information results in better-controlled performance. In a feature-based visual feedback system, using redundant features may be useful to improve the robustness and controlled performance. However, since the feature-based approach tries to regulate all features, redundant features causes the controllability problem. Although Weiss *et al.* [6] and Feddema *et al.* [7], [8] studied how to choose the features so that the feedback information was sufficiently rich, no attempt have been so far made at the controllability problem caused by using redundant features.

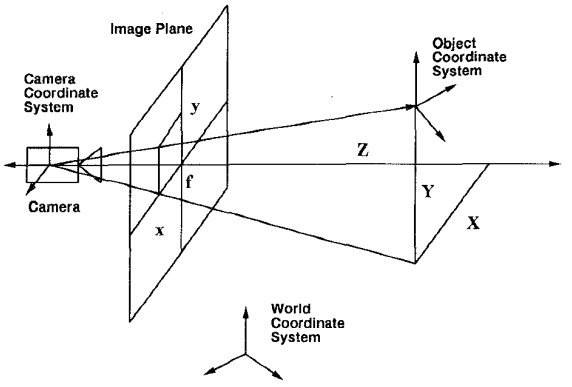

Fig. 2. Perspective imaging model.

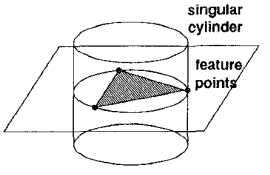

Fig. 3. Singular cylinder.

A. Perspective Imaging Model and Image Jacobian

Take an ideal perspective transformation as the imaging model with f being the focal length of the lens, as shown in Fig. 2. The image of the object positioned at $[X\ Y\ Z]^T$ in the camera coordinate system becomes

$$\begin{bmatrix} x \\ y \end{bmatrix} = \frac{f}{Z}\begin{bmatrix} X \\ Y \end{bmatrix}. \tag{1}$$

Differentiating both sides yields [15], [16]

$$\begin{bmatrix} \dot{x} \\ \dot{y} \end{bmatrix} = J_{\text{image}}(x, y, Z)\begin{bmatrix} {}^c v_c \\ {}^c \omega_c \end{bmatrix} \tag{2}$$

where

$$J_{\text{image}}(x, y, Z) \stackrel{\text{def}}{=} \begin{bmatrix} -\frac{f}{Z} & 0 & \frac{x}{Z} & \frac{xy}{f} & -\frac{x^2+f^2}{f} & y \\ 0 & -\frac{f}{Z} & \frac{y}{Z} & \frac{y^2+f^2}{f} & -\frac{xy}{f} & -x \end{bmatrix} \tag{3}$$

and ${}^c v_c$ and ${}^c \omega_c$ are the linear and angular velocities of the camera with respect to the camera coordinate system. The matrix J_{image} is called the *image Jacobian*. Combining (1) for N points, namely, $[x_1\ y_1]^T, \cdots, [x_N\ y_N]^T$, yields

$$\dot{\xi} = J^+_{\text{image}}(\xi, Z)\begin{bmatrix} {}^c v_c \\ {}^c \omega_c \end{bmatrix} \tag{4}$$

where

$$J^+_{\text{image}}(\xi, Z) \stackrel{\text{def}}{=} \begin{bmatrix} J_{\text{image}}(x_1, y_1, Z_1) \\ \vdots \\ J_{\text{image}}(x_N, y_N, Z_N) \end{bmatrix} \tag{5}$$

$\xi = [x_1\ y_1 \cdots x_N\ y_N]^T$ and $Z = [Z_1\ Z_2 \cdots Z_N]^T$. The matrix J^+_{image} is called the *extended image Jacobian* and the vector ξ is called the *feature vector*. We should avoid the *degenerated features*, i.e., the features that do not move if the camera moves. For the degenerated features ξ_a there exists at least a nonzero vector a that satisfies

$$0 = J^+_{\text{image}}(\xi_a, Z)a. \tag{6}$$

Thus to avoid the degenerated features, the features should be selected so that the extended image Jacobian becomes full rank. To make the Jacobian full rank, $N \geq 3$ is an obvious necessary condition. If $N = 3$ the Jacobian loses the rank if the camera lies on the cylinder which includes the three points and the axis of which is perpendicular to the plane containing these points [17] (see Fig. 3). Moreover, image noise may cause the Jacobian to become nearly singular. Thus $N \geq 4$ is desirable for the feature-based visual servoing. If $N \geq 4$, the object position and orientation can be uniquely defined by the feature vector ξ [18].

B. LTI Model

Define the state and the control input of the visual feedback system as $\xi = [x_1\ y_1 \cdots x_N\ y_N]^T$ and $u = [{}^c v_c^T\ {}^c \omega_c^T]^T$, respectively. To derive the LTI model, we expand $\dot{\xi}$ in (4) for a power series around the desired state ξ_d. Let u_d be the desired input which keeps the system at the equilibrium point $\xi \equiv \xi_d$. For simplicity of notation, we define a function η by

$$\eta(\xi, Z, u) \stackrel{\text{def}}{=} \dot{\xi} = J^+_{\text{image}}(\xi, Z)u. \tag{7}$$

Noting that Z is a function of ξ and expanding η around ξ_d and u_d yields

$$\eta = \eta_d + \left(\frac{\partial \eta_d}{\partial \xi} + \frac{\partial \eta_d}{\partial Z}\frac{\partial Z_d}{\partial \xi}\right)\bar{\xi} + \frac{\partial \eta_d}{\partial u}\bar{u} \tag{8}$$

where $\eta_d \stackrel{\text{def}}{=} \eta(\xi_d, Z_d, u_d)$ is the time derivative of the features at the desired point, $Z_d \stackrel{\text{def}}{=} Z(\xi_d)$ is the desired depth, $\bar{\xi} \stackrel{\text{def}}{=} \xi_d - \xi$ is the state error and $\bar{u} \stackrel{\text{def}}{=} u - u_d$ is the input disturbance. Letting η_i and u_i be the ith element of η and u, respectively, and J_{ij} be the ijth element of $J^+_{\text{image}}(\xi, Z)$ gives $\eta_i = \sum_{j=1}^m J_{ij}u_j$. Thus the partial derivatives in (8) are given by

$$\frac{\partial \eta_i}{\partial \xi} = \sum_{j=1}^m u_j \frac{\partial}{\partial \xi}J_{ij}, \quad \frac{\partial \eta_i}{\partial Z} = \sum_{j=1}^m u_j \frac{\partial}{\partial Z}J_{ij}$$
$$\frac{\partial \eta_i}{\partial u} = [J_{i1} \cdots J_{im}]. \tag{9}$$

Note, if the system is at an equilibrium point, the input u should be zero because the matrix $J^+_{\text{image}}(\xi, Z)$ has full column rank. Therefore, the partial derivatives evaluated at the desired equilibrium point are given by

$$\frac{\partial \eta_d}{\partial \xi} = 0, \quad \frac{\partial \eta_d}{\partial Z} = 0 \quad \text{and} \quad \frac{\partial \eta_d}{\partial u} = J^+_{\text{image}}(\xi_d, Z_d). \tag{10}$$

Consequently, the following LTI error model is derived:

$$\frac{d}{dt}\bar{\xi} = J^+_{\text{image}}(\xi_d, Z_d)u. \tag{11}$$

The discretized model with T being the sampling period is given by

$$\bar{\xi}(k+1) = \bar{\xi}(k) + Bu(k) \tag{12}$$

where k stands for the time index and $B \stackrel{\text{def}}{=} TJ^+_{\text{image}}(\xi_d, Z_d)$. Note that the rank of the controllability matrix is equal to the rank of B. Thus if $N \geq 4$, the system is not controllable because the size of the state vector is $2N(\geq 8)$ and the rank of the controllability matrix is smaller than 6. However, if the desired feature is defined properly, the input u which makes the error vanish should exist. To understand this inconsistency, note that the state variables can not move independently because the all features are on an object and the object is rigid. Since the state-space model allows each state variable to move independently, we have to put some restriction on the state vector which will be explained in the next section.

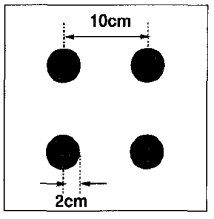

Fig. 4. Configuration of feature points.

III. LQ Optimal Control Law

In this section we introduce the controllable and uncontrollable modes of the feature error vector. On the basis of the LTI model (12), a design procedure of the feedback controller which minimizes an LQ type performance criterion is proposed. The problem is formulated to find the control input $u(k)$ that minimizes the performance criterion

$$J = \sum_{k=0}^{\infty} (\bar{\xi}^T(k) Q \bar{\xi}(k) + u^T(k) R u(k)) \tag{13}$$

where Q and R are symmetric positive definite weighting matrices introduced to put penalties on the state error $\bar{\xi}$ and the control input u, respectively. The conventional approach does not work well because the system (12) is, in appearance, uncontrollable. However, by making two natural assumptions, we can prove that the error converges to the zero vector and thus the summation of the right hand of (13) exists and is finite.

A. Controllability

Let $\theta = [\theta_1, \ldots, \theta_6]^T$ be the vector of joint angles. The assumptions are as follows.

1) Assumption 1 (Object Rigidness): For the given static and rigid object there exists ψ, a function of θ, which generates the image features of the object ξ such that

$$\xi = \psi(\theta). \tag{14}$$

2) Assumption 2 (Soundness of the Desired Features): For the given ξ_d, there exists a set of joint angles θ_d that achieves the desired features:

$$\xi_d = \psi(\theta_d) \tag{15}$$

where the function ψ is defined in (14).

Assumption 1 states that the degree of freedom of the feature vector reduces to that of the robot manipulator. Assumption 2 is essential to achieve the desired image by moving the robot hand. Therefore, these two assumptions are essential for visual servoing with redundant features.

Before proving the controllability of (12) we define the neighborhood of the point θ_d by

$$N(\gamma) = \{\theta : (\psi(\theta) - \xi_d)^T (\psi(\theta) - \xi_d) < \gamma\}. \tag{16}$$

We should choose γ so that the following conditions hold:

$$\forall \theta \in N(\gamma),\ \det[B^T J^+_{\text{image}}(\psi(\theta), Z(\psi(\theta)))] \neq 0$$

and

$$\det[{}^c J_{\text{robot}}(\theta)] \neq 0 \tag{17}$$

where ${}^c J_{\text{robot}}$ is the *robot Jacobian* defined by

$${}^c J_{\text{robot}} \stackrel{\text{def}}{=} \frac{\partial}{\partial \theta} \begin{bmatrix} {}^c v_c \\ {}^c \omega_c \end{bmatrix}. \tag{18}$$

Using these preliminaries, we will show the following theorem.

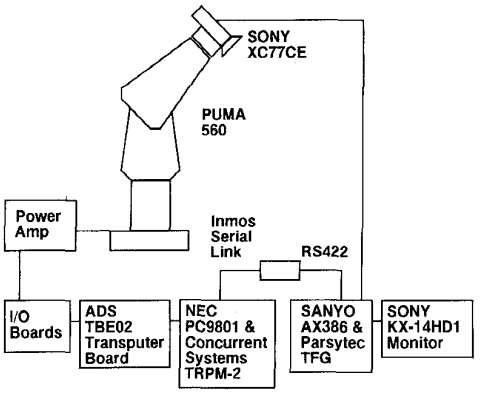

Fig. 5. Visual feedback control system.

Theorem 1 (Local Reachability of ξ_d): For the given θ_d and $\xi_d = \psi(\theta_d)$, fix a positive number γ which satisfies (17). Then, for every initial joint angle $\theta(0) \in N(\gamma)$, the desired feature vector ξ_d is reachable under some control input u.

Proof: We prove the theorem by actually constructing the feedback input u. For the system (12), since the matrix B has full column rank, there exists a $2N \times 2N$ orthonormal matrix S satisfying

$$SB = \begin{bmatrix} B_c \\ 0 \end{bmatrix} \quad \text{and} \quad SS^T = I \tag{19}$$

where B_c is a 6×6 nonsingular matrix. Premultipling S to (12) yields

$$\begin{bmatrix} \bar{\xi}_c(k+1) \\ \bar{\xi}_u(k+1) \end{bmatrix} = \begin{bmatrix} \bar{\xi}_c(k) \\ \bar{\xi}_u(k) \end{bmatrix} + \begin{bmatrix} B_c \\ 0 \end{bmatrix} u(k) \tag{20}$$

where $\bar{\xi}_c$ and $\bar{\xi}_u$ are, respectively, the six-dimensional and $2N-6$-dimensional vectors which are defined by

$$\begin{bmatrix} \bar{\xi}_c(k) \\ \bar{\xi}_u(k) \end{bmatrix} \stackrel{\text{def}}{=} S\bar{\xi}(k). \tag{21}$$

Equation (20) shows that $\bar{\xi}_c$ is controllable and $\bar{\xi}_u$ is uncontrollable. Thus the state decomposition defined by (21) is called controllable/uncontrollable mode decomposition. Now, since the matrix B_c is not singular, we can choose an appropriate 6×6 gain matrix K_c such that the following characteristic polynomial

$$\det(zI - I + B_c K_c) = 0 \tag{22}$$

has all solutions inside the unit circle. By using this K_c, the state feedback control law

$$u = -[K_c \ \ 0] \begin{bmatrix} \bar{\xi}_c \\ \bar{\xi}_u \end{bmatrix} = -[K_c \ \ 0] S\bar{\xi} \tag{23}$$

yields the response

$$\begin{bmatrix} \bar{\xi}_c(k) \\ \bar{\xi}_u(k) \end{bmatrix} = \begin{bmatrix} (I - B_c K_c)^k & 0 \\ 0 & I \end{bmatrix} S\bar{\xi}(0) \tag{24}$$

where $\bar{\xi}(0) = \xi(0) - \xi_d$ is the initial error. Since $\bar{\xi}^T(0)\bar{\xi}(0) < \gamma$, we have $\bar{\xi}^T(k)\bar{\xi}(k) < \gamma$ for all $k \geq 0$. Therefore, $\theta(k) \in N(\gamma)$ for all k. Letting the final error be $\bar{\xi}_\infty$ yields

$$B^T \bar{\xi}_\infty = [B_c^T \ \ 0] SS^T \begin{bmatrix} 0 \\ \bar{\xi}_u \end{bmatrix} = 0. \tag{25}$$

The mean value theorem guarantees the existence of $\tilde{J}$ such that

$$\bar{\xi}_\infty = \xi(\infty) - \xi_d = \psi(\theta(\infty)) - \psi(\theta_d) = \tilde{J}(\theta(\infty) - \theta_d). \tag{26}$$

Since the conditions (17) holds, we can conclude that $\theta(\infty) = \theta_d$, which yields, from Assumption 2, $\xi(\infty) = \xi_d$. Consequently, the

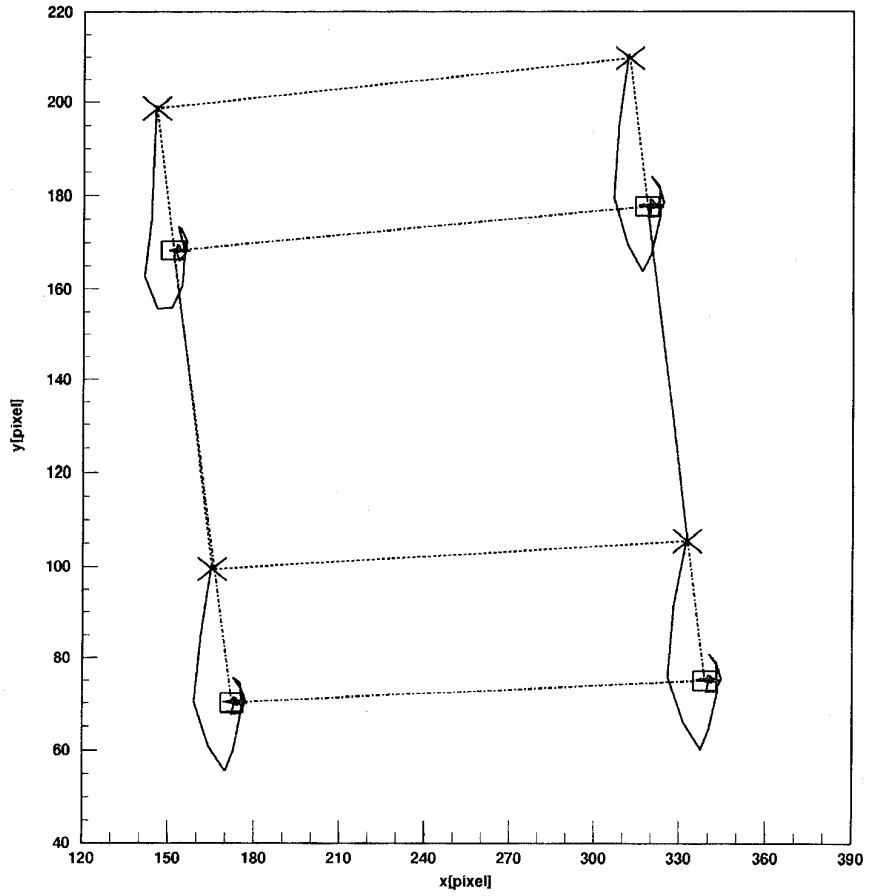

Fig. 6. Trajectory of 4 points (translation). ×: Initial position, □: Reference.

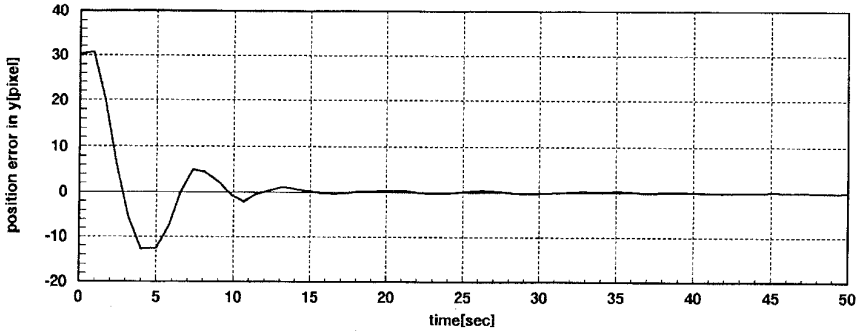

Fig. 7. Error plot of a point (translation).

system (12) with state feedback (23) is asymptotically stable if all the eigenvalues of the matrix $I - B_c K_c$ are in the unit circle. □

On the basis of Theorem 1 and its proof, one can state the following corollary.

Corollary 1 (Asymptotical Stability of ξ_d): Under Assumptions 1 and 2, ξ_d is asymptotically stable with state feedback $u = -K\bar{\xi}$ if the six eigenvalues of $I - BK$ are inside the unit circle (the other eigenvalues are always 1).

The asymptotical stability is proved only in the neighborhood of ξ_d. However, the deviations on B will not affect the stability provided the six eigenvalues of $I - BK$ stay inside the unit circle. Therefore, the LTI approach is valid for considerably large range of object motions.

B. Controller Design

The next problem is the design of the gain matrix K_c. The above discussion shows that $\bar{\xi}_u \equiv 0$. Thus the system becomes

$$[\bar{\xi}_c(k+1)] = \begin{bmatrix} \bar{\xi}_c(k) \\ 0 \end{bmatrix} + \begin{bmatrix} B_c \\ 0 \end{bmatrix} u(k). \tag{27}$$

Therefore, minimization of the performance criterion

$$\begin{aligned} J &= \sum_{k=0}^{\infty} (\bar{\xi}^T(k) Q \bar{\xi}(k) + u^T(k) R u(k)) \\ &= \sum_{k=0}^{\infty} (\bar{\xi}_c(k) Q_c \bar{\xi}_c(k) + u^T(k) R u(k)) \end{aligned} \tag{28}$$

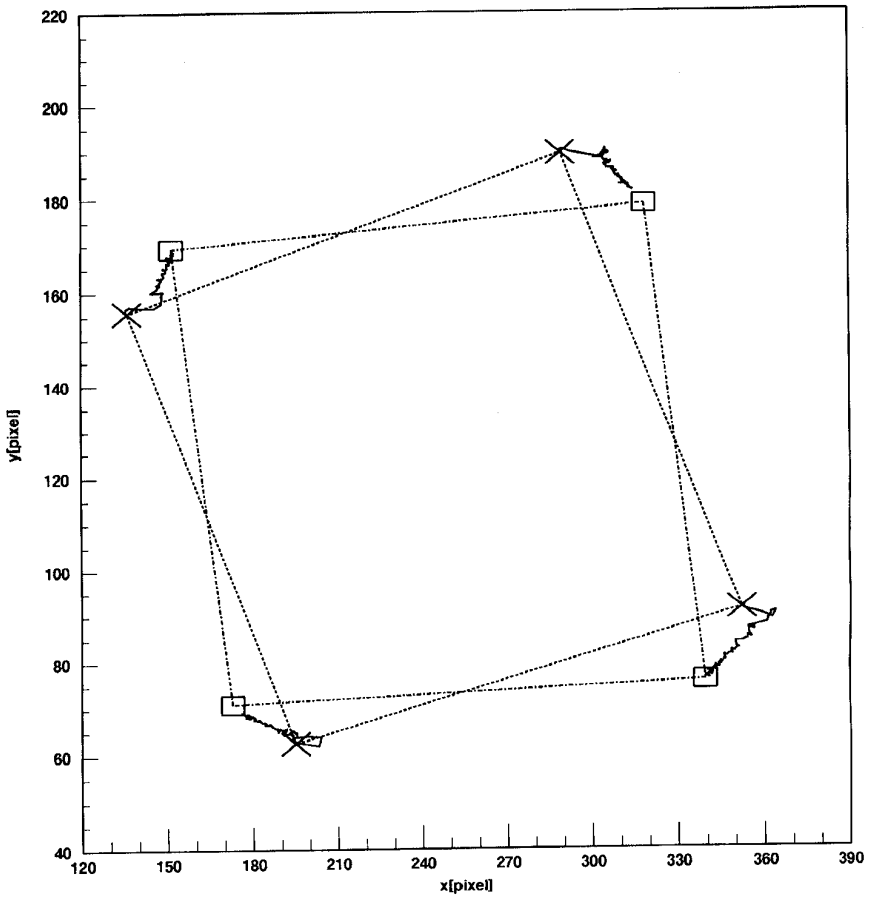

Fig. 8. Trajectory of 4 points (rotation). ×: Initial position, □: Reference.

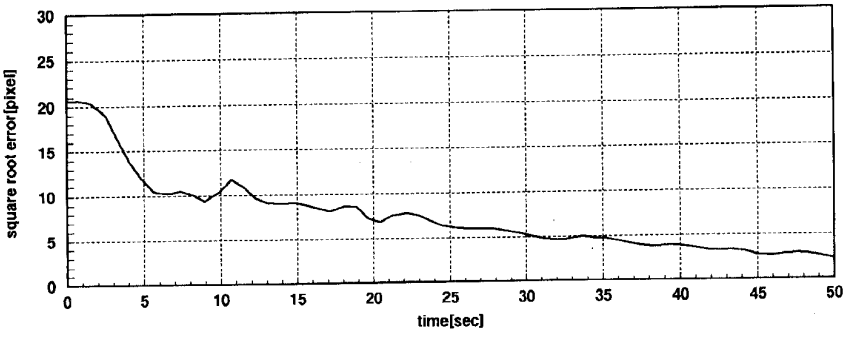

Fig. 9. Error plot of a point (rotation).

where

$$\begin{bmatrix} Q_c & * \\ * & * \end{bmatrix} = SQS^T \tag{29}$$

can be achieved by the state feedback

$$\begin{aligned} u &= -K_c\bar{\xi}_c = -[K_c \;\; 0]S\bar{\xi} \\ K_c &= (R + B_c^T P B_c)^{-1} B_c^T P \end{aligned} \tag{30}$$

where P is the 6×6 symmetric, positive definite matrix satisfying the discrete time algebraic Riccati equation

$$Q_c = PB_c(R + B_c^T P B_c)^{-1} B_c^T P. \tag{31}$$

The weighting matrices Q and R in (28) are the parameters to be used to tune the control performance. Note that, since the matrix B_c depends on the choice of the state transformation matrix S which satisfies (19), the feedback gain $K = -[K_c \;\; 0]S$ seems to depend on S. However, we can prove the following theorem.

Theorem 2 (Independence of K From the Choice of S): For the given B, the feedback gain K that minimizes the performance index J does not depend on the choice of S.

Proof: Let S_1 and S_2 be the upper 6 and lower $2N - 6$ rows of the matrix S

$$\begin{bmatrix} S_1 \\ S_2 \end{bmatrix} \stackrel{\text{def}}{=} S. \tag{32}$$

Then, from (19), we have

$$\mathcal{R}(B) = \mathcal{R}(S_1^T) \quad \text{and} \quad \mathcal{N}(B^T) = \mathcal{R}(S_2^T) \tag{33}$$

where $\mathcal{R}$ and $\mathcal{N}$ stand for the range space and null space, respectively. Another choice of the state transformation matrix, say, $\tilde{S}$, also satisfies

$$\mathcal{R}(B) = \mathcal{R}(\tilde{S}_1^T) \quad \text{and} \quad \mathcal{N}(B^T) = \mathcal{R}(\tilde{S}_2^T) \tag{34}$$

where

$$\tilde{S} = \begin{bmatrix} \tilde{S}_1 \\ \tilde{S}_2 \end{bmatrix}, \quad \tilde{S}B = \begin{bmatrix} \tilde{B}_c \\ 0 \end{bmatrix}, \quad \text{and} \quad \tilde{S}\tilde{S}^T = I. \tag{35}$$

Equations (34) and (35) show that each row of $\tilde{S}_1$ ($\tilde{S}_2$) is the linear combinations of the row vectors of S_1 (S_2). Therefore, $\tilde{S}$ is parameterized by

$$\begin{bmatrix} \tilde{S}_1 \\ \tilde{S}_2 \end{bmatrix} = \begin{bmatrix} T_1 & 0 \\ 0 & T_2 \end{bmatrix} \begin{bmatrix} S_1 \\ S_2 \end{bmatrix}, \quad T_1 T_1^T = I_6 \quad \text{and} \quad T_2 T_2^T = I_{2N-6} \tag{36}$$

where I_6 and I_{2N-6} are the 6 and $2N-6$ dimensional identity matrices, respectively. Choosing $\tilde{S}$, instead of S, gives the feedback gain

$$\begin{aligned} \tilde{K} &= -[\tilde{K}_c \;\; 0]\tilde{S} = -[(R + \tilde{B}_c^T \tilde{P} \tilde{B}_c)^{-1} \tilde{B}_c^T \tilde{P} \;\; 0]\tilde{S} \\ &= -[(R + B_c^T T_1^T \tilde{P} T_1 B_c)^{-1} B_c^T T_1^T \tilde{P} T_1 \;\; 0]S \end{aligned} \tag{37}$$

where $\tilde{P}$ is the unique solution of the following discrete time Riccati equation:

$$\begin{aligned} \tilde{Q}_c &= \tilde{P}\tilde{B}_c(R + \tilde{B}_c^T \tilde{P} \tilde{B}_c)^{-1} \tilde{B}_c \tilde{P} \\ &= \tilde{P} T_1 B_c (R + B_c^T T_1^T \tilde{P} T_1 B_c)^{-1} B_c^T T_1^T \tilde{P} \end{aligned} \tag{38}$$

and $\tilde{Q}_c$ is defined by

$$\begin{bmatrix} \tilde{Q}_c & * \\ * & * \end{bmatrix} = \tilde{S}\tilde{Q}\tilde{S}^T. \tag{39}$$

Since (39) gives $\tilde{Q}_c = T_1 Q_c T_1^T$, the solution of (38) is given by $\tilde{P} = T_1 P T_1^T$ and, thus, we obtain $\tilde{K} = K$. Consequently, the gain matrix is independent of the choice of S. □

Throughout this research, since the feedback gain K does not depend on the choice of S, we use the singular value decomposition

$$B = U \begin{bmatrix} \Sigma \\ 0 \end{bmatrix} V^T \tag{40}$$

to choose S and B_c by

$$S = U^T \quad \text{and} \quad B_c = \Sigma V^T. \tag{41}$$

IV. Experiments

As shown in Fig. 4, the object is a white board with four black marks. Features are selected as the x and y coordinates of the center of the image of each mark. The task is specified to move the camera so that the relative position between the camera and object are kept constant. Two cases of step input experiments are performed to show the quick response of the system. Translational and rotational steps are separately examined to verify that our design specification is reflected in the performance. Moreover, experimental examples of object tracking are carried out to evaluate the flexibility of the controller design of the LQ approach.

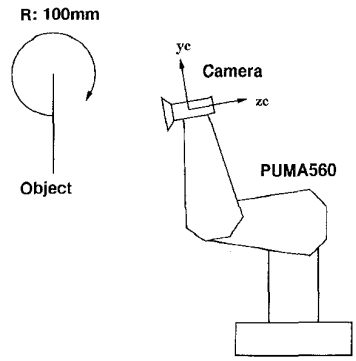

Fig. 10. Setup for tracking experiment.

A. Robot Control System Configuration

We have developed a visual feedback control system depicted in Fig. 5. The host computer for vision system is a personal computer (AX386) with an image processing board (whose processing unit is a Transputer) added in. The host computer for the manipulator control is a personal computer (PC9801) with a Transputer board added in. The parallel computation scheme of the resolved motion rate control is implemented on a network of eight Transputers (TBE02).

The I/O boards are consist of an interface board to communicate with the Transputer and with AD/DA/Counter boards, AD boards to input the potentiometer reading values, DA boards to output the command torque, and counter boards to input the encoder reading values. We designed and implemented all interface circuits. A CCD video camera (XC77CE) is mounted on the end-effector of the PUMA 560 arm. The internal calibration of the camera and the external calibration of the geometrical relationship between the camera and the end-effector are carried out based on the calibration algorithm proposed by Tsai and Lenz [18].

The sampling period of the vision system is 85 ms. The sampling period of the manipulator control is fixed to 1ms. The commanded camera motion ${}^c v_c$ and ${}^c w_c$ computed at the image processing board are sent to the robot controller every 85 ms. The motion command are interpolated and fed to the Transputer network every 1 ms.

B. Translational Motion

The response of the feature points in the image plane is shown in Fig. 6. The initial feature vector is $\xi(0) = [146, 198, 312, 209, 333, 105, 165, 99]^T$. The desired feature vector is $\xi_d = [151, 168, 318, 178, 339, 75, 172, 70]^T$. The weighting matrices are $Q = 300 I_8$ and $R = \mathrm{diag}(1.0, 1.0, 1.0, 6.0, 6.0, 6.0)$, where I_8 is the 8×8 identity matrix. The penalties on the rotational components are six times larger than that of the translational components because our objective is to track the translational motion of the object. If the rotational penalties are small, the object motion is first tracked by the pitch motion of the wrist and afterward the arm gradually moves to decrease the orientation error.

To show the speed of the response, a plot of a feature point is shown in Fig. 7. Overshoot is found but the response is fast (15 s to stabilize). Because of the pipeline architecture of the image processing board, the closed loop system has delay of 1 visual sampling time (85 ms). Thus the higher feedback gains cause oscillations and the response times are not improved. The smaller gains which has closed loop eigenvalues close to the real axis can achieve a little quicker response. However, this gain is selected by putting importance on the tracking performance shown in Section IV-D.

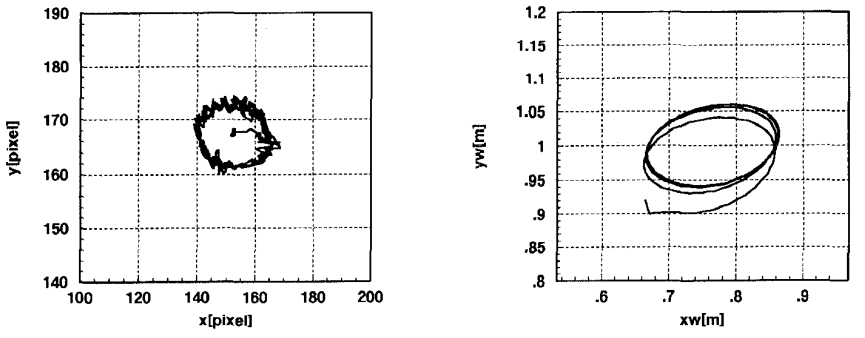

(a) (b)

Fig. 11. Experimental results with optimal regulator. (a) Trajectory of a feature point (left). (b) Camera position (right) $R = I_6$, $Q = 300I_8$, Speed = 5 r/min.

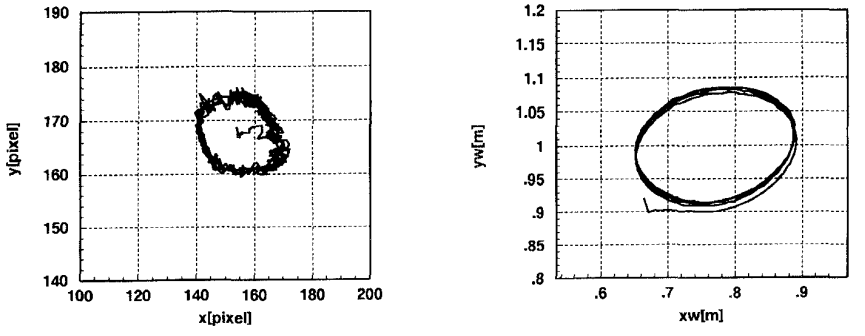

(a) (b)

Fig. 12. Experimental results with optimal regulator. (a) Trajectory of a feature point (left). (b) Camera position (right). $R = \text{diag}(1.0, 1.0, 0.5, 6.0, 6.0, 6.0)$, $Q = 300I_8$, Speed = 5 r/min.

Although the step in this experimentation is small (20 pixels≈200 mm) due to the limitations of the vision processor, the stability test of Corollary 1 shows that the same gain can stabilize the object motion smaller than 3000 mm.

C. Rotational Motion

Another experiment is done for rotational step change of the reference position. The initial feature vector is $\xi(0) = [136, 155, 290, 189, 353, 90, 195, 62]^T$. The desired feature vector is $\xi_d = [152, 169, 319, 179, 340, 76, 173, 71]^T$. The rotation angle is about 10 deg. The sampling period and the controller parameters are the same as that of the last experiment. We put large penalties on the rotational motion of the camera because we want to track the object motion with the arm motion (not the wrist motion). Thus the speed of the rotation should be very slow. Fig. 8 shows the step response of the feature points in the image plane. It is clearly shown that all points converges to the reference points.

To verify the speed of convergence Fig. 9 shows the step response of one of the feature points in the image plane. The vertical axis is the square root error in pixel. The sluggish convergence verifies that our design specification of the controller is well reflected to the performance. If the penalties on the rotational motion are small the speed is improved.

Although the step of this experimentation is small (10 deg) due to the image processing limitations, the test of Corollary 1 shows that the same gain can stabilize the object rotation smaller than 60 deg.

D. Tracking

As depicted in Fig. 10, the object moves along a circle of radius 0.1 m in the y_c–z_c plane of the camera coordinate system, i.e., the x_w–y_w plane of the world coordinate system. The object moves translationally. The task is to track a moving object with the camera mounted on the hand so that the relative position and orientation are kept constant. Note that this object motion includes depth change and thus camera motion in the optical axis direction is required to track the object. In the image plane, the feature points move in the direction of the vertical axis. The speed of the motion is 5 r/min. Experimental results are shown in Figs. 11 and 12.

Fig. 11(a) and (b) shows the results with optimal regulator ($R = I_6$, $Q = 300I_8$). Fig. 11(a) shows the trajectory of a feature point in the image plane. The desired position is [153, 167]. The tracking error is smaller than 20 pixels in the x direction, and smaller than 10 pixels in the y direction. Fig. 11(b) shows the camera position in the world coordinate system. The desired trajectory is a circle of radius 0.1 m with the center at $[0.763, 0.997]$. The tracking accuracy in the x_w direction is good, but the motion in the y_w direction is somewhat smaller than the desired one. The reason is that the object motion in the y_w direction (up and down) is tracked by the camera's up and down motion as well as the camera's orientation change, i.e., by the pitch motion of the manipulator wrist.

To suppress the wrist rotation and encourage the up and down motion, another R is selected which has smaller penalty on the $z_c (= y_w)$ directional movement and larger penalty on the rotational movement, $R = \text{diag}(1.0, 1.0, 0.5, 6.0, 6.0, 6.0)$. Q is $300I_8$. The object speed is 5 r/min. The experimental result is shown in Fig. 12(a) and (b). As depicted in Fig. 12(a), the feature point tracking error is almost the same as that of the previous experiment [Fig. 11(a)]. Fig. 12(b) shows that the camera tracking performance is fairly improved. This experiment shows that the controller performance tuning is quite easy. This is a favorable characteristic of the optimal control method.

V. Conclusion

A control theoretic formulation for the visual feedback system was proposed. On the basis of the formulation, discrete time LTI MIMO model was derived. Discussions on the controllability were presented. The controllability problem caused by redundant features was resolved by introducing the controllable and uncontrollable modes decomposition. If the object is a static rigid body and the desired features are achievable, the LTI model was proved to be asymptotically stable with an appropriate choice of the gain matrix. An efficient way of designing the gain matrix based on the LQ performance index was proposed. The controller is computationally effective because none of real-time computation of depth, image Jacobian and its inverse is required. Real-time experiments on PUMA 560 were carried out to evaluate the optimal approach. The results have shown the validity of the LTI model as well as the LQ controller design method. Also they showed the quickly converging stable performance of the proposed LQ controller. The performance improvement was done easily by selecting the weighting matrices.

However, the robustness and the accuracy of the redundant feature system are not shown. Also the dynamics of the manipulator, which is highly nonlinear and important for fast motions, is not considered in the LTI model proposed in this paper. Thus, study on the robustness, dynamic effect and design of nonlinear controller are left as the next research subject.

Acknowledgment

The authors thank the reviewers for their valuable comments.

References

[1] Y. Shirai and H. Inoue, "Guiding a robot by visual feedback in assembly tasks," *Patt. Recogn.*, vol. 5, pp. 99–108, 1973.

[2] R. S. Ahluwalia and L. M. Fogwell, "A modular approach to visual servoing," in *IEEE Int. Conf. Robotics and Automation*, San Francisco, CA, 1987, pp. 943–950.

[3] A. J. Koivo and N. Houshangi, "Real-time vision feedback for servoing robotic manipulator with self-tuning controller," *IEEE Trans. Syst., Man, Cybern.*, vol. 21, no. 1, pp. 134–142, 1991.

[4] P. K. Allen, A. Timcenko, B. Yoshimi and P. Michelman, "Automated tracking and grasping of a moving object with a robotic hand-eye system," *IEEE Trans. Robot. Automat.*, vol. 9, no. 2, pp. 152–165, 1993.

[5] W. J. Wilson, "Visual servo control of robots using Kalman filter estimates of relative pose," in *12th IFAC World Congress*, Sydney, Australia, 1993, vol. 9, pp. 399–404.

[6] L. E. Weiss, A. C. Sanderson and C. P. Newman, "Dynamic sensor-based control of robots with visual feedback," *IEEE J. Robot. Automat.*, vol. RA-3, no. 5, pp. 404–417, 1987.

[7] J. T. Feddema and O. R. Michell, "Vision guided servoing with feature-based trajectory generation," *IEEE Trans. Robotics and Automation*, vol. 5, no. 5, pp. 691–700, 1989.

[8] J. T. Feddema, C. S. G. Lee and O. R. Michell, "Weighted selection of image features for resolved rate visual feedback control," *IEEE Trans. Robot. Automat.*, vol. 7, no. 1, pp. 31–47, 1991.

[9] N. Papanikolopoulos, P. K. Khosla and T. Kanade, "Visual tracking of a moving target by a camera mounted on a robot: A combination of control and vision," *IEEE Trans. Robot. Automat.*, vol. 9, no. 1, pp. 14–35, 1993.

[10] N. Papanikolopoulos and P. K. Khosla, "Adaptive robotic visual tracking: Theory and experiments," *IEEE Trans. Automat. Contr.*, vol. 38, no. 3, pp. 429–445, 1993.

[11] B. Espiau, F. Chaumette, and P. Rives, "A new approach to visual servoing in robotics," *IEEE Trans. Robot. Automat.*, vol. 8, no. 3, pp. 313–326, 1992.

[12] W. Jang and Z. Bien, "Feature-based visual servoing of an eye-in-hand robot with improved tracking performance," in *IEEE Int. Conf. Robotics and Automation*, Sacramento, CA, 1991, pp. 2254–2260.

[13] K. Hashimoto, "Model-based control of a manipulator with image-based dynamic visual servo," Ph.D. dissertation, Osaka Univ., Japan, 1991.

[14] K. Hashimoto *et al.*, "Image-based dynamic visual servo for a hand-eye manipulator," in *MTNS-91*, Kobe, Japan, pp. 609–614, 1991.

[15] H. Longuet-Higgins and K. Prazdny, "The interpretation of a moving retinal image," in *Proc. Royal Soc. London Ser. B*, 1984, vol. 208, pp. 385–397.

[16] K. Hashimoto *et al.*, "Manipulator control with image-based visual servo," in *IEEE Int. Conf. Robotics and Automation*, Sacramento, CA, 1991, pp. 2267–2272.

[17] H. Michel and P. Rives, "Singularities in the determination of the situation of a robot effector from the perspective view of 3 points," INRIA, 1993, Tech. Rep. 1850.

[18] R. Y. Tsai and R. K. Lenz, "A new technique for fully autonomous 3D robotic hand/eye calibration,"*IEEE Trans. Robot. Automat.*, vol. 5, no. 3, pp. 345–358, 1989.